Shape changes and large-amplitude collective dynamics in neutron-rich Cr isotopes

Kenichi Yoshida and Nobuo Hinohara

RIKEN Nishina Center for Accelerator-Based Science, Wako, Saitama 351-0198, Japan

(Dated: January 18, 2013)

Shape-phase transition in neutron-rich Cr isotopes around $N = 40$ is investigated by employing the collective Hamiltonian approach. The inertial functions for large-amplitude vibration and rotation are evaluated by the local normal modes along the axial quadrupole collective coordinate using the Skyrme and pairing energy density functionals. The time-odd components of the mean fields are fully included in the derived masses. The low-lying spectra obtained by requantizing the collective Hamiltonian show an excellent agreement with the recent experimental data. Gradual change from spherical to axially deformed shapes in between $N = 34$ and 38 is well described.

How can we define the shape of quantum many-body systems? Atomic nuclei have a variety of equilibrium shapes, and show shape changes along the isotopic or isotonic chain. The mean-field approximation gives us an intuitive picture of the nuclear shape. However, we have to go beyond it to describe the shape-phase transition; the dynamical change of the mean-field potential associated with the large-amplitude collective motion.

The self-consistent mean-field model employing the effective interaction or the nuclear energy-density-functional (EDF) method has successfully described the ground-state properties [1]. Recent advances in the computing capability together with the highly-developed techniques in the nuclear EDF method allow us to calculate the ground-state properties of nuclei including deformation in the entire mass region of the nuclear chart [2].

Magic number or shell closure is an essential concept in understanding the stability against the deformation. The subshell closure at 40 created by the gap between $1g_{9/2}$ and $2p_{1/2}, 1f_{5/2}$ orbitals has attracted much attention for several reasons [3]. The proton-rich $N = Z$ nucleus ^{80}Zr lies in the center of the well-deformed $A \simeq 80$ region [4]. This is because a shell gap of 40 again appears in a deformed region, and the shell effect of protons and neutrons coherently stabilize the nucleus deformed. On the other hand, the existence of $N = 40$ subshell closure is suggested experimentally for the neutron-rich nucleus ^{68}Ni [5, 6]. The strength of this subshell closure and its persistence for $Z < 28$ determine the waiting point for the r-process nucleosynthesis at ^{64}Cr, which is considered to be a progenitor of ^{64}Ni [7].

The half-life measurement at CERN-ISOLDE have deduced that the neutron-rich ^{66}Fe is deformed with a quadrupole deformation $\beta \sim 0.26$ [8]. Since the Cr isotopes lie at mid proton $1f_{7/2}$ shell, protons could additionally destabilize the nucleus in a spherical shape and favor deformation. Experimental evidences of the nuclear shape changes are related to low-lying quadrupole collectivity, such as the small excitation energy of the 2_1^+ state, the ratio of the excitation energy of the 2_1^+ and 4_1^+ states $R_{4/2} = E_{4+}/E_{2+}$, and the reduced transition probability $B(E2; 2_1^+ \rightarrow 0_1^+)$, etc. The observed small excitation energy of the 2_1^+ state in neutron-rich Cr isotopes indicates that the deformation develops toward $N = 40$ [9–13].

Very recently, the large-scale shell-model calculation for the neutron-rich Cr isotopes has become available [14], where the Hamiltonian with dimension of $\sim 10^{10}$ is diagonalized. However, deducing the picture of deformation is difficult in the fully quantum-mechanical calculations.

In this article, on the basis of the nuclear EDF method closely related to the mean-field approximation, we develop a new framework of the microscopic theory for the large-amplitude collective motion employing the quadrupole collective Hamiltonian approach for the axially-symmetric nuclei. The similar attempts of the EDF-based collective Hamiltonian starting from the Gogny interaction [15, 16], the relativistic Lagrangian [17, 18] and the Skyrme interaction [19] have been made for description of the large-amplitude collective motion. The cranking approximation, however, has been applied to calculate the inertial functions [15–19], and the time-odd components of the mean field remain largely unexplored except for a few attempts in the adiabatic time-dependent Hartree-Fock-Bogoliubov theories [20–22]. Our method includes the time-odd mean fields in the inertial functions. And this method is applied to the shape-phase transition in neutron-rich Cr isotopes around $N = 40$.

We start from the $(1 + 2)$D (vibration along the β direction and rotations about the two axes which are perpendicular to the symmetry axis) quadrupole collective Hamiltonian;

$$\mathcal{H}_{\mathrm{coll}} = \frac{1}{2}\mathcal{M}_\beta(\beta)\dot{\beta}^2 + \frac{1}{2}\sum_{i=1}^{2}\mathcal{J}_i(\beta)\omega_i^2 + V(\beta). \quad (1)$$

With the Pauli's prescription, we requantize Eq. (1) and construct the collective Schrödinger equation;

$$\hat{H}_{\mathrm{coll}}\Psi_{\alpha IM}(\beta, \theta_1, \theta_2) = E_{\alpha I}\Psi_{\alpha IM}(\beta, \theta_1, \theta_2), \quad (2)$$

where $\Psi_{\alpha IM}(\beta, \theta_1, \theta_2)$ is the collective wave functions in the laboratory frame, I is the angular momentum quan-

tum number, M is the $z-$component of I, and $E_{\alpha I}$ is the excitation energy. The collective wave functions are written in terms of wave functions in the body-fixed frame $\Phi_{\alpha IK}(\beta)$;

$$\Psi_{\alpha IM}(\beta, \Omega) = \sum_{K=0}^{I} \Phi_{\alpha IK}(\beta)\langle\Omega|IMK\rangle = \Phi_{\alpha I}(\beta)\langle\Omega|IM0\rangle, \quad (3)$$

with $\langle\Omega|IMK\rangle$ a superposition of the rotational wave functions.

The collective Schrödinger equation in the intrinsic frame now reads

$$\left\{\hat{T}_{\text{vib}} + \frac{I(I+1)}{2\mathcal{J}(\beta)} + V(\beta)\right\}\Phi_{\alpha I}(\beta) = E_{\alpha I}\Phi_{\alpha I}(\beta), \quad (4)$$

where

$$\hat{T}_{\text{vib}} = -\frac{1}{2M_\beta(\beta)}\frac{\partial^2}{\partial\beta^2}$$
$$+ \frac{1}{2M_\beta(\beta)}\left[\frac{1}{2M_\beta(\beta)}\frac{\partial M_\beta(\beta)}{\partial\beta} - \frac{1}{\mathcal{J}(\beta)}\frac{\partial\mathcal{J}(\beta)}{\partial\beta}\right]\frac{\partial}{\partial\beta}, \quad (5)$$

and the vibrational wave function is normalized as

$$\int d\beta \Phi_{\alpha I}^*(\beta)\Phi_{\alpha' I}(\beta)|G(\beta)|^{1/2} = \delta_{\alpha\alpha'} \quad (6)$$

with the metric $|G(\beta)| = M_\beta(\beta)\mathcal{J}^2(\beta)$.

The collective potential $V(\beta)$ is calculated by solving the constrained Hartree-Fock-Bogoliubov (CHFB) equation;

$$\delta\langle\phi(\beta)|\hat{H}_{\text{CHFB}}|\phi(\beta)\rangle = 0, \quad (7)$$

$$\hat{H}_{\text{CHFB}} = \hat{H} - \sum_\tau \lambda^\tau \hat{N}^\tau - \mu\hat{Q}_{20}. \quad (8)$$

The microscopic Hamiltonian $\hat{H}$ is constructed from the Skyrme and pairing EDFs. Following the discussion in Ref. [23], the vibrational mass $M_\beta(\beta)$ is evaluated using the local normal mode as

$$M_\beta(\beta) = \frac{1}{\eta^2}\frac{\partial q_\beta}{\partial Q_{20}}\frac{\partial q_\beta}{\partial Q_{20}}, \quad (9)$$

$$\frac{\partial Q_{20}}{\partial q_\beta} = \frac{\partial}{\partial q_\beta}\langle\phi(\beta)|\hat{Q}_{20}|\phi(\beta)\rangle = \langle\phi(\beta)|[\hat{Q}_{20}, \frac{\hat{P}^\beta}{i}]|\phi(\beta)\rangle \quad (10)$$

by solving the local quasiparticle-random-phase approximation (LQRPA) equation on top of the CHFB state $|\phi(\beta)\rangle$;

$$\delta\langle\phi(\beta)|[\hat{H}_{\text{CHFB}}, \hat{Q}_\nu] - \frac{\hat{P}^\nu}{i}|\phi(\beta)\rangle = 0, \quad (11)$$

$$\delta\langle\phi(\beta)|[\hat{H}_{\text{CHFB}}, \frac{\hat{P}^\nu}{i}] - \omega_\nu^2\hat{Q}_\nu|\phi(\beta)\rangle = 0, \quad (12)$$

$$\langle\phi(\beta)|[\hat{Q}_\mu, \frac{\hat{P}^\nu}{i}]|\phi(\beta)\rangle = \delta_\mu^\nu. \quad (13)$$

Here, the isoscalar quadrupole moment operator $\hat{Q}_{20}$ and $\eta = \sqrt{\pi}/\sqrt{5}A\langle r^2\rangle$ are calculated at each state $|\phi(\beta)\rangle$. We write the collective coordinate as q_β. The rotational moment of inertia $\mathcal{J}(\beta)$ is evaluated by the LQRPA equation for collective rotation (extension of Thouless-Valatin equation to CHFB states [23]).

The reduced quadrupole matrix elements used for calculating the $E2$ transition probability and the spectroscopic quadrupole moment are evaluated as

$$\langle\alpha I||E2||\alpha'I'\rangle = \sqrt{(2I+1)(2I'+1)}(-)^I$$
$$\begin{pmatrix} I & 2 & I' \\ 0 & 0 & 0 \end{pmatrix}\langle\alpha I|\hat{F}_{E2}|\alpha'I'\rangle, \quad (14)$$

$$\langle\alpha I|\hat{F}_{E2}|\alpha'I'\rangle = \int d\beta\Phi_{\alpha I}^*(\beta)F_{E2}(\beta)\Phi_{\alpha'I'}(\beta)|G(\beta)|^{1/2}, \quad (15)$$

where $F_{E2}(\beta) = \langle\phi(\beta)|\hat{F}_{E2}|\phi(\beta)\rangle$, and $\hat{F}_{E2}$ is the electric quadrupole moment operator.

We solve the CHFB plus LQRPA equations employing the extended procedures of Refs. [25, 26]. To describe the nuclear deformation and the pairing correlations simultaneously with a good account of the continuum, we solve the CHFB equations in the coordinate space using cylindrical coordinates $\boldsymbol{r} = (\rho, z, \phi)$ with a mesh size of $\Delta\rho = \Delta z = 0.5$ fm and a box boundary condition at $(\rho_{\max}, z_{\max}) = (12.25, 12.00)$ fm. We assume axial and reflection symmetries for the CHFB states. The quasiparticle (qp) states are truncated according to the qp energy cutoff at $E_\alpha \leq 60$ MeV. We introduce the additional truncation for the LQRPA calculation, in terms of the two-quasiparticle (2qp) energy as $E_\alpha + E_\beta \leq 60$ MeV. In the present calculation, the LQRPA equations are solved on top of around 20 CHFB states. For each LQRPA calculation, we employ 256 CPUs and it takes about 185 CPU hours to calculate the inertial functions. Thus, for construction of the collective Hamiltonian, it takes about 3 700 CPU hours for each nucleus.

For the normal (particle-hole) part of the EDF, we employ the SkM* functional [24], and for the pairing energy, we adopt the volume-type pairing interaction as in Ref. [27], where the deformation mechanism in neutron-rich Cr isotopes is investigated in detail.

Figure 1 shows the total energy curves (collective potentials) of neutron-rich Cr isotopes under investigation. In ^{58}Cr and ^{60}Cr, the potentials are soft against the β deformation even we get the HFB minima at $\beta = 0$. Beyond $N = 38$, the prolate minimum gradually develops up to $N = 44$. We can see a shoulder or a shallow minimum at the oblately deformed region as well. It is noted that the systematic calculation predict ^{74}Cr is spherical due to the magicity at $N = 50$ [2] using the same EDF as in the present calculation.

Figure 2 shows the properties of low-lying states. When the neutron number increases from ^{58}Cr, the excitation energy of the 2_1^+ state drops toward ^{62}Cr. The
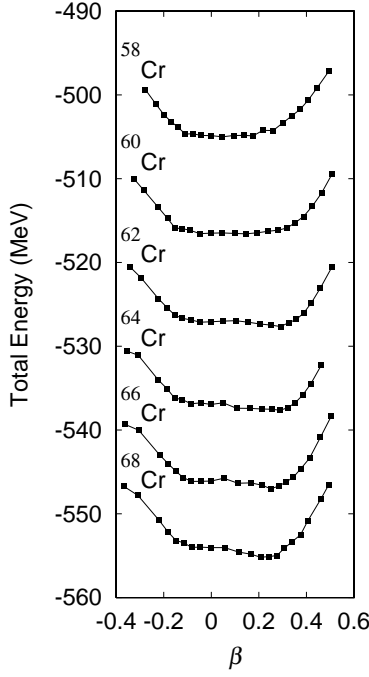
FIG. 1: Total energy curves of neutron-rich Cr isotopes calculated with SkM* and volume pairing interactions.

$R_{4/2}$ ratio and the transition probability $B(E2; 0_1^+ \rightarrow 2_1^+)$ grow up at the same time. Although we overestimate $E(2_1^+)$ at $N = 34$, these features are consistent with the experimental results [11–13], and it clearly shows the onset of deformation at $N \sim 38$. The experimental $B(E2)$ value is available only in ^{58}Cr [10]. The present calculation underestimates the observation. Underestimation of the quadrupole collectivity of ^{58}Cr probably attributes to the restriction of the collective coordinate to the β and two rotational degree of freedom and/or to the EDF employed in the present calculation.

Let us consider here the simplified case in solving Eq. (4) with a harmonic oscillator potential and a constant vibrational mass;

$$V(\beta) = \frac{1}{2}C\beta^2, M_\beta(\beta) = B, \mathcal{J}(\beta) = 3B\beta^2. \quad (16)$$

We obtain $E(2_1^+) = 2.00$ MeV and $E(4_1^+) = 4.26$ MeV, when we adopt $B = 50$ MeV^{-1} and $C = 200$ MeV. The exact value for $E(2_1^+)$ is $\omega = \sqrt{C/B} = 2$ MeV and $E(4_1^+) = 2\omega = 4$ MeV in the full five-dimensional collective Hamiltonian. This simple exercise implies that the present $(1+2)$D collective Hamiltonian can describe reasonably well the vibrational spectra of spherical nuclei. However, the $B(E2; 2_1^+ \rightarrow 0_1^+)$ value in the $(1+2)$D model is $3/5$ times as large as an exact one. Therefore, in (nearly) spherical nuclei, all the five quadrupole degrees of freedom should be treated on the same footing, and it remains as future work.
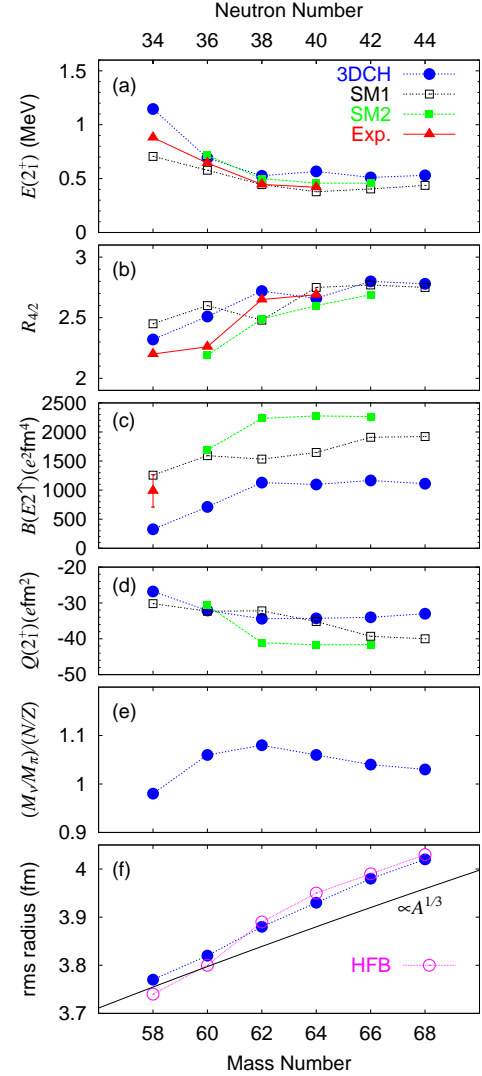

FIG. 2: (Color online) (a): Excitation energies of the 2_1^+ state in Cr isotopes. (b): Ratios of the $E(4_1^+)$ to $E(2_1^+)$. (c): Reduced transition probabilities $B(E2; 0_1^+ \rightarrow 2_1^+)$. (d): Spectroscopic quadrupole moment of the 2_1^+ state. (e): Ratios of the transition matrix elements of neutrons to protons divided by the neutron to proton numbers. (f): Root-mean-square matter radii. Experimental data are taken from Refs. [10–13]. Results of the shell-model calculations (denoted as SM1 [28] and SM2 [14]) are also included.

The results of the spherical shell-model calculations employing the pairing-plus-multipole forces with the monopole correction [28] and the LNPS interaction [14] are also shown in Fig. 2. Lowering of $E(2_1^+)$ toward $N = 38$ is consistent with the experiments and with the present calculation.

We show in Fig. 2(e) the ratios of the matrix elements of neutrons to protons M_ν/M_π divided by the neutron to proton numbers for the excitation to the 2_1^+ state. If the neutrons and protons coherently contribute to the excitation mode, M_ν/M_π may approach N/Z. We can see
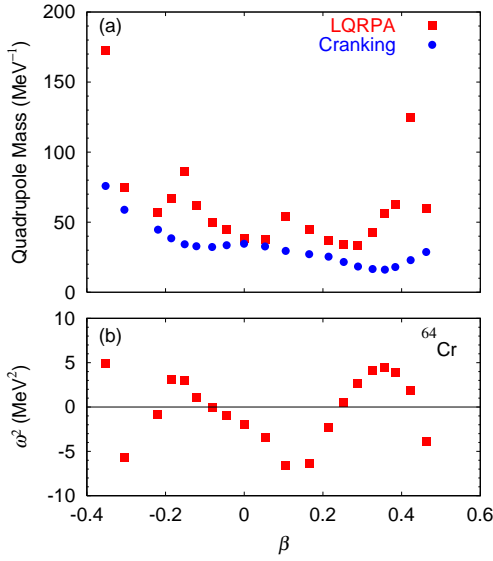
FIG. 3: (Color online) (a): Quadrupole masses calculated by the LQRPA and the cranking formula in ^{64}Cr. (b): Excitation energies squared for the associated collective modes.

FIG. 4: (Color online) Collective wave functions of the $I^{\pi} = 0_1^+$ state in Cr isotopes.

that the neutron excitation develops from $N = 34$ to 38 associated with the increase of the quadrupole collectivity.

Evolution of deformation is also seen in the matter radii as shown in Fig. 2(f). For the reference, we show the $A^{1/3}$ dependence and the HFB results by a solid line and open circles, respectively. In the deformed systems, the increase of radius is proportional to β^2. Thus, beyond $N = 38$ the radius is constantly larger than the systematics of $A^{1/3}$. Furthermore, we can see that the calculated radius is larger than the HFB result in ^{58}Cr and ^{60}Cr associated with the large-amplitude fluctuation.

It is interesting to compare our results with those in Ref. [16], where the collective Hamiltonian approach is also employed. In Ref. [16], they employ the five-dimensional collective Hamiltonian, in which both the β and γ degrees of freedom are included. And the D1S-Gogny EDF is used for the particle-hole and particle-particle parts of the energy density. The rotational mass is evaluated by the Inglis-Belyaev procedure, and the vibrational mass is calculated by use of the cranking approximation [15]. In Ref. [16], they obtained for ^{64}Cr $E(2_1^+) = 0.82$ MeV, $R_{4/2} = 2.2$, $Q(2_1^+) = -34$ efm^2, and $B(E2 \uparrow) = 1515$ e^2fm^4. The $B(E2)$ value and $Q(2_1^+)$ are similar to our results, whereas $E(2_1^+)$ and $E(4_1^+)$ are rather larger. With the D1S-Gogny EDF, there is still a clear minimum at the spherical point, and a shallow local minimum around $\beta = 0.3$ [16].

In our approach, the time-odd components of the mean field are fully included for the calculation of the collective masses. Figure 3(a) shows the calculated vibrational masses along the collective coordinate. The col-
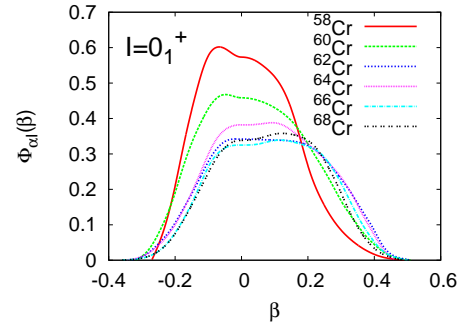
lective masses calculated by use of the cranking approximation are also shown, where the time-odd components are neglected. The cranking masses show a smooth behavior as functions of the deformation β. This is because the cranking mass is evaluated by combination of the sum-rule values. In contrast to the cranking masses, the LQRPA masses strongly depend on the deformation, microscopic structure of the collective mode. And the LQRPA masses are larger than the cranking masses. In Fig. 3(b), the excitation energies squared ω_i^2 of the collective modes are shown. This quantity represents the curvature of the collective potential as seen in Eq. (12). The two-humped structure is associated with the existence of the two minima in the collective potential of ^{64}Cr.

Finally, we discuss the shape evolution of the ground state. Figure 4 shows the vibrational wave functions of the 0_1^+ state. In ^{58}Cr, the wave function is distributed around $\beta = 0$. But the wave functions is not sharply localized at the spherical minimum of the potential, which reflects the softness of the collective potential against the deformation. When two neutrons are added to ^{58}Cr, broadening of the wave function can be seen. When two more neutrons are added, the wave function moves toward a prolately deformed minimum with a large spreading. From this figure, we can say that ^{60}Cr is located close to the critical point of the shape-phase transition in neuron-rich Cr isotopes and the large-amplitude dynamics plays a dominant role.

In summary, we have developed a new framework of the microscopic model for the large-amplitude collective motion based on the nuclear EDF method. The collective masses and the potential appearing in the quadrupole collective Hamiltonian are evaluated employing the constrained HFB and local QRPA approach, where the time-odd components of the mean field are fully taken into account. The microscopic Hamiltonian is constructed from the Skyrme and the pairing EDFs.

We applied this new framework to the shape-phase transition in neutron-rich Cr isotopes around $N = 40$.

The present calculation gives consistent results for the low-lying excited states with the observations and the other theoretical approaches. Investigating the collective wave functions, we reach a conclusion that ^{60}Cr is located close to the critical point of the shape phase transition, and the onset of deformation takes place at $N = 38$. The large-amplitude dynamics plays a dominant role in the shape changes in neutron-rich Cr isotopes.

As a future work, it would be interesting to compare the present framework with the generator-coordinate method using the β-constrained HFB states. And the systematic investigation of the properties of low-lying collective states such as $E(2_1^+)$, $R_{4/2}$ and $B(E2)$ in the entire region of nuclear chart is quite challenging both in nuclear structure physics and in computational science as a large-scale calculation employing the massively-parallel supercomputers.

[1] M. Bender, P-H. Heenen and P-G. Reinhard, Rev. Mod. Phys. **75**, 121 (2003).
[2] M. V. Stoitsov, J. Dobaczewski, W. Nazarewicz, S. Pittel, and D. J. Dean, Phys. Rev. C **68**, 054312 (2003), and http://massexplorer.org/.
[3] P.-G. Reinhard, D. J. Dean, W. Nazarewicz, J. Dobaczewski, J. A. Maruhn, M. R. Strayer, Phys. Rev. C **60**, 014316 (1999).
[4] W. Nazarewicz, J. Dudek, R. Bengtsson, T. Bengtsson, and I. Ragnarsson, Nucl. Phys. **A435**, 397 (1985).
[5] R. Broda *et al.*, Phys. Rev. Lett. **74**, 868 (1995).
[6] O. Sorlin *et al.*, Phys. Rev. Lett. **88**, 092501 (2002).
[7] O. Sorlin *et al.*, Nucl. Phys. **A660**, 3 (1999).
[8] M. Hannawald *et al.*, Phys. Rev. Lett. **82**, 1391 (1999).
[9] O. Sorlin *et al.*, Eur. Phys. J. A **16**, 55 (2003).
[10] A. Bürger *et al.*, Phys. Lett. **B622**, 29 (2005).
[11] S. Zhu *et al.*, Phys. Rev. C **74**, 064315 (2006).
[12] N. Aoi *et al.*, Phys. Rev. Lett. **102**, 012502 (2009).
[13] A. Gade *et al.*, Phys. Rev. C **81**, 051304R (2010).
[14] S. M. Lenzi, F. Nowacki, A. Poves, and K. Sieja, Phys. Rev. C **82**, 054301 (2010).
[15] J. Libert, M. Girod, and J.-P. Delaroche, Phys. Rev. C **60**, 054301 (1999).
[16] L. Gaudefroy *et al.*, Phys. Rev. C **80**, 064313 (2009).
[17] T. Nikšić, Z. P. Li, D. Vretenar, L. Próchniak, J. Meng, and P. Ring, Phys. Rev. C **79**, 034303 (2009).
[18] Z. P. Li, T. Nikšić, D. Vretenar, and J. Meng, Phys. Rev. C **81**, 034316 (2010).
[19] L. Próchniak and S. G. Rohoziński, J. Phys. G: Nucl. Part. Phys. **36**, 123101 (2009).
[20] J. Dobaczewski and J. Skalski, Nucl. Phys. **A369**, 123 (1981).
[21] M. J. Giannoni and P. Quentin, Phys. Rev. C **21**, 2060 (1980).
[22] M. J. Giannoni and P. Quentin, Phys. Rev. C **21**, 2076 (1980).
[23] N. Hinohara, K. Sato, T. Nakatsukasa, M. Matsuo, and K. Matsuyanagi, Phys. Rev. C **82**, 064313 (2010).
[24] J. Bartel, P. Quentin, M. Brack, C. Guet, and H.-B. Håkansson, Nucl. Phys. **A386**, 79 (1982).
[25] K. Yoshida and N. V. Giai, Phys. Rev. C **78**, 064316 (2008).
[26] K. Yoshida and T. Nakatsukasa, Phys. Rev. C **83**, 021304R (2011).
[27] H. Oba and M. Matsuo, Prog. Theor. Phys. **208**, 143 (2008).
[28] K. Kaneko, Y. Sun, M. Hasegawa, and T. Mizusaki, Phys. Rev. C **78**, 064312 (2008).